6

Alternative Surface Integral Equation Formulations

The discussion of surface integral equations in Chapters 1 and 2 avoided one potential problem with these formulations. When used to describe exterior electromagnetic scattering problems, certain surface integral equations may not produce unique solutions if applied to closed geometries that also represent resonant cavities. This chapter explores the numerical consequences of the uniqueness problem and considers several remedies.

6.1 UNIQUENESS OF SOLUTIONS TO THE EXTERIOR SURFACE EFIE AND MFIE [1]

An EFIE formulation for the scattering of a TM plane wave from an infinite, perfectly conducting cylinder was discussed in Section 2.1. The EFIE is given by

$$E_z^{\text{inc}}(t) = jk\eta \int J_z(t') \frac{1}{4j} H_0^{(2)}(kR)\, dt' \tag{6.1}$$

where

$$R = \sqrt{[x(t) - x(t')]^2 - [y(t) - y(t')]^2} \tag{6.2}$$

and t is a parametric variable along the cylinder surface. Although this surface integral equation can be applied to a cylinder of arbitrary cross-sectional shape, consider the special case of a circular cylinder. Comparisons presented in Section 2.1 demonstrated excellent agreement between numerical and exact solutions for circular cylinders. However, consider Figure 6.1, which presents the numerical solution for the magnitude of the surface current density induced on a cylinder with $ka = 2.405$. The numerical result obtained using the procedure of Section 2.1 with 40 basis and testing functions differs appreciably from the exact solution. Interestingly, if we increase the order of the discretization by adding additional basis and testing functions, the results do not improve. The behavior of the

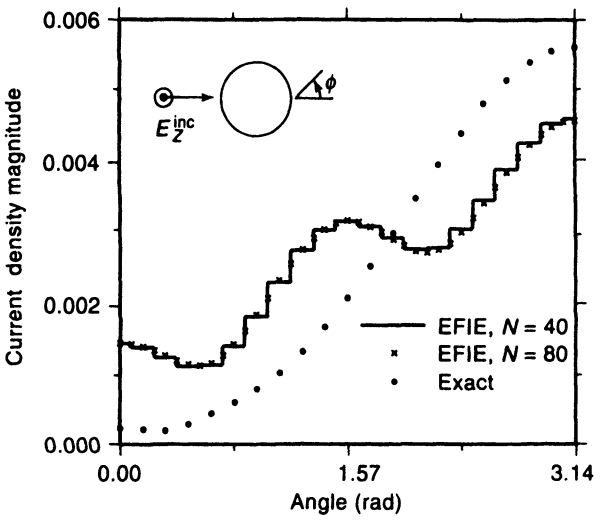

Figure 6.1 Magnitude of the surface current density produced by two discretizations of the TM EFIE for a circular cylinder with $ka = 2.405$ illuminated by a uniform plane wave. The exact solution is shown for comparison.

numerical solution is symptomatic of a fundamental difficulty with certain surface integral formulations. For reasons that will soon be apparent, the difficulty has come to be known as the *interior resonance* problem.

To understand the source of the difficulty in this example, recall the discussion in Chapter 5 concerning eigenfunctions and eigenvalues of integral operators. It was shown that the eigenfunctions of the TM EFIE operator for circular cylinders are the exponential functions $\{e^{jn\phi}\}$. Analytical expressions for the eigenvalues of the EFIE as a function of the cylinder radius a are given as

$$\lambda_n^{\text{EFIE,TM}} = \tfrac{1}{2}(\eta\pi ka) J_n(ka) H_n^{(2)}(ka) \tag{6.3}$$

where J_n and H_n denote the Bessel and Hankel functions of order n. A plot of the eigenvalues of orders 0, 1, and 2 as a function of ka is presented in Figure 5.7. For small values of ka (low-frequency excitation), the eigenvalues cluster at the origin. As ka increases, each eigenvalue moves in a circularlike path that passes through the origin at various nonzero values of ka. From Equation (6.3), it is clear that the eigenvalues vanish at the zeros of the Bessel function $J_n(ka)$.

What is the effect of a zero eigenvalue? In short, it means that any multiple of the corresponding eigenfunction can be added to the solution and still satisfy the equation. This eigenfunction is a source-free or homogeneous solution. Consequently, whenever $J_n(ka)$ vanishes in (6.3), the EFIE does not have a unique solution. Although the EFIE was constructed in order to represent the exterior scattering problem, the equation also admits interior cavity fields as homogeneous solutions. The root of the problem is that the surface integral equation only involves data on the mathematical surface of the scatterer and cannot distinguish between "inside" and "outside" in order to produce the desired exterior solution. The interior geometry represented by this EFIE is the circular cavity having perfect electric walls. Since nonzero cavity fields can occur only when $J_n(ka) = 0$, the EFIE has unique solutions at other frequencies.

For geometries that cannot be treated analytically (basically anything other than circular cylinders), we employ the method of moments to convert a surface integral equation into a finite-dimensional matrix equation. As a consequence of the manner in which eigenvalues are projected from a continuous operator onto a matrix operator during discretization

(Section 5.7), at values of ka where an eigenvalue of the integral operator vanishes, an eigenvalue of the matrix operator will also become very small. If the matrix eigenvalue is zero to machine precision, any multiple of the corresponding eigenvector will satisfy the matrix equation. When this occurs, the matrix is singular and cannot be inverted or factorized into the LU form. If the eigenvalue is nonzero but very small, the matrix is nearly singular. It is no surprise that numerical solutions become less stable under these conditions. In fact, since Figure 6.1 illustrates the behavior of the numerical solution when $ka = 2.405$, near the first zero of J_0 in Equation (6.3), error in the solution might be expected.

Similar behavior can be observed with an MFIE formulation. Section 2.2 discussed the MFIE representing the scattering of a TE wave from a perfectly conducting cylinder. The equation has the form

$$-H_z^{\text{inc}}(t) = J_t(t) + \hat{z} \cdot \nabla \times \int \hat{t}(t') J_t(t') \frac{1}{4j} H_0^{(2)}(kR) dt' \tag{6.4}$$

For the special case of a circular cylinder, the eigenfunctions of the MFIE operator are also the exponential functions $\{e^{jn\phi}\}$. Analytical expressions for the eigenvalues corresponding to these eigenfunctions are

$$\lambda_n^{\text{MFIE,TE}} = \tfrac{1}{2}(j\pi ka) J_n(ka) H_n^{(2)\prime}(ka) \tag{6.5}$$

where the prime denotes differentiation with respect to the argument of the Hankel function. A plot of the eigenvalues of order 0, 1, and 2 is presented in Figure 5.9. Note that the character of the MFIE eigenvalues differs from that of the EFIE eigenvalues (Figure 5.7). For small ka, the MFIE eigenvalues cluster at 0.5 or 1.0 in the right-half complex plane. However, as ka increases, these eigenvalues move in a circularlike path, in common with the EFIE eigenvalues, and occasionally pass through the origin. As indicated by Equation (6.5), the MFIE eigenvalues also vanish at the zeros of the Bessel function $J_n(ka)$. These values of ka represent the frequencies where source-free solutions exist for the interior problem, which in this case is a circular cavity having walls that are perfect magnetic conductors.

Figure 6.2 shows the magnitude of the surface current density obtained from a numerical solution of the MFIE near $ka = 2.405$ using the approach of Section 2.2. When compared to the exact solution, we observe that the numerical solution for the surface current density contains considerable error. The bistatic scattering cross section computed from these currents is shown in Table 6.1 and is grossly inaccurate.

For the example illustrated in Figure 6.2, the numerical results produced by our specific implementation are incorrect within a frequency range spanning approximately $2.401 < ka < 2.409$. Since the original integral operator has a zero eigenvalue at the resonance frequency $ka \cong 2.405$, one might expect to find that the matrix is singular at that frequency. However, this is not the case. Although an eigenvalue of the matrix approaches the origin near this frequency, the matrix condition number (see Chapter 4) computed for our implementation remains below 100. Because of discretization error, the matrix remains nonsingular and the equation apparently has a unique solution over the entire frequency range. In fact, numerical experimentation demonstrates that the incorrect numerical results displayed in Figures 6.1 and 6.2 are actually very stable. As the order of the discretization is improved (more basis and testing functions), the results appear to converge to some solution. This solution, however, is clearly not the desired solution to the exterior scattering problem. In other words, the numerical solution is incorrect, but not because of ill-conditioning or numerical round-off errors.

To understand the nature of the incorrect numerical solution, consider the magnitude of the surface current density produced by the TM EFIE at $ka = 2.405$, as displayed in

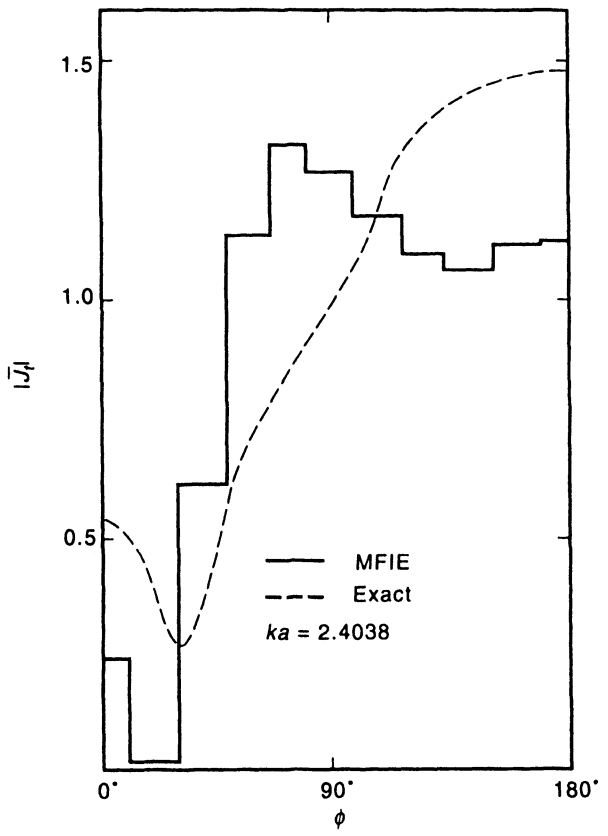

Figure 6.2 Comparison of the MFIE and exact solutions for the TE current density on a circular cylinder of radius $0.3826\lambda_0$. After [1]. ©1990 Hemisphere Publishing Corporation.

TABLE 6.1 Bistatic Scattering Cross Section for Circular Cylinder of Circumference 2.4038

	Scattering Cross Section (dBλ)	
Bistatic Angle (deg)	MFIE	Exact
0	-2.49	3.46
30	-2.70	0.90
60	+2.51	0.98
90	-3.17	-3.68
120	-13.4	-0.72
150	-6.34	0.68
180	-6.42	0.17

Note: The MFIE result obtained using 20 pulse basis functions is corrupted by an internal resonance. The scattering cross section computed from the incorrect MFIE current density is compared with the exact solution.

Figure 6.1. The exact solution for the surface current density produced by a uniform plane wave can be written as [2]

$$J_z(\phi) = \frac{-2}{\eta\pi ka} \sum_{n=-\infty}^{\infty} j^{-n} \frac{1}{H_n^{(2)}(ka)} e^{jn\phi} \tag{6.6}$$

Numerical experimentation suggests that as the discretization is refined, the difference between the exact and numerical result at $ka = 2.405$ converges to

$$J_{\text{exact}}(\phi) - J_{\text{numerical}}(\phi) = \frac{-2}{\eta\pi ka} \frac{1}{H_0^{(2)}(ka)} \tag{6.7}$$

In other words, the numerical result is correct except for the magnitude of the resonant eigenfunction (in this case, $e^{j0\phi}$). This is as expected, since, in theory, the original integral equation would admit any multiple of this eigenfunction [i.e., $J_z(\phi) = K_0 e^{j0\phi}$ for any K_0] as a solution at resonance. What is initially surprising is that the numerical solution apparently suppressed this eigenfunction completely. Instead of producing solutions with unstable and wildly varying coefficients of the resonant eigenfunction, as might be expected, the matrix equation consistently produced a stable solution having zero for the coefficient K_0.

Two observations help explain the stability of the incorrect solution for this example. First, the discretization error associated with the matrix operator prevents the eigenvalue corresponding to the resonant eigenfunction from being as small as that of the original integral operator. This is apparent from the matrix condition number, which does not exceed several hundred in our implementation. The second observation involves the excitation employed in the problem. For the TM EFIE, a plane-wave incident electric field on the surface of the circular cylinder can be written as

$$E_z^{\text{inc}}(\rho = a, \phi) = \sum_{n=-\infty}^{\infty} j^{-n} J_n(ka) e^{jn\phi} \tag{6.8}$$

Because of the factor $J_n(ka)$, the component of the zeroth resonant eigenfunction in the excitation vanishes when ka is approximately 2.405. The eigenvalue appearing in Equation (6.3) also contains the factor $J_0(ka)$, which in an analytical solution exactly cancels the $J_0(ka)$ of the excitation. However, discretization error perturbs the matrix eigenvalue from the exact analytical eigenvalue in the vicinity of the first zero of $J_0(ka)$. For our implementation, the matrix eigenvalue is larger than the exact eigenvalue in magnitude, and the matrix solution tends to suppress the resonant eigencurrent. The numerical solution for surface current density is incorrect because of the improper balance between the tangential component of the excitation and the nearly resonant eigencurrent. In fact, the solution will only be correct if these two factors precisely cancel.

Although the difficulty in this example appears to be a consequence of numerical limitations, it is actually of a more fundamental nature. In fact, *there is not enough information contained in the tangential incident electric field on the scatterer surface at resonance to determine the true current density*. This observation is apparent from Equation (6.8). Although the zero harmonic of the tangential incident electric field vanishes at the cylinder surface, it does not vanish within the cylinder and requires some component of surface current to properly cancel the interior incident field. Additional information not contained in the tangential incident electric field on the surface is necessary to determine the proper weighting of the zero harmonic when $J_n(ka) = 0$.

The numerical behavior depends somewhat on the specific approximations employed. In addition to the discretization error introduced with the basis and testing functions, the matrix entries computed for the preceding examples contained some error due to approximations made in evaluating the integrals. These errors affect the precise location of the matrix eigenvalues. A more accurate evaluation of these integrals should improve the balance between the excitation and the matrix eigenvalue and reduce the frequency range over which the incorrect numerical behavior is observed. At the same time, improved accuracy should increase the condition number of the matrix near resonance and introduce the possibility that the matrix will appear singular to machine precision at resonance. On the other hand, if the entries of the excitation column vector are not accurately computed, it is possible that the matrix eigenvalue might be smaller in magnitude than the corresponding coefficient in the excitation. Under these circumstances, the coefficient of the resonant eigencurrent can be large and the resonant eigencurrent will not be suppressed in the numerical solution. Since the excitation entries do not require an integration over a singular Green's function, however, they are likely to be computed more accurately than the matrix eigenvalue in practice.

As observed in Figure 6.1, suppressing the resonant eigencurrent introduces significant error into the surface current density. However, because the resonant eigencurrent produced by the EFIE does not radiate exterior to the scatterer, the far-zone fields should not be affected by the incorrect weighting of that eigencurrent. In other words, accurate far fields can sometimes be computed from the incorrect EFIE surface current density.

The TE MFIE exhibits a similar behavior in the vicinity of an interior resonance. A uniform plane-wave incident magnetic field used with Equation (6.4) can be expressed as

$$H_z^{\text{inc}}(\rho = a, \phi) = \sum_{n=-\infty}^{\infty} j^{-n} J_n(ka) e^{jn\phi} \tag{6.9}$$

This field has the same form as Equation (6.8), and the coefficient of the eigenfunction $e^{jn\phi}$ vanishes whenever ka is a zero of $J_n(ka)$. Since the MFIE of (6.4) only involves the z-component of the incident field, no information is available to properly specify the resonant eigencurrent when $J_n(ka)$ vanishes. In common with the EFIE formulation, a nonzero resonant eigencurrent must be present in order to properly cancel the incident field within the cylinder. The consequence of the incorrect eigencurrent is severe in the case of the MFIE because the resonant eigencurrent does radiate and will significantly alter the far fields (Table 6.1 and Prob. P6.1). Thus, it is usually impossible to compute accurate far fields from a corrupted solution of the MFIE.

We have considered circular cylinder examples because of the ease in identifying analytical expressions for the eigenvalues of the EFIE and MFIE operators. For general scatterer shapes, incorrect numerical solutions occur whenever the scatterer surface is closed and coincides with a resonant cavity. (Solutions of the EFIE are incorrect near the resonant frequencies of cavities having perfect electric walls; solutions of the MFIE degrade near the resonant frequencies of cavities having perfect magnetic walls.) In practice, it is not trivial to predict in advance whether an arbitrary closed surface happens to coincide with a resonant cavity. However, because a matrix eigenvalue becomes relatively small near an internal resonance, abrupt changes in the matrix condition number can be used to identify probable resonant frequencies. For instance, Figure 6.3 shows the matrix condition number returned by the LINPACK LU factorization algorithm CGECO for the TE MFIE circular cylinder example. The sharp peaks in the graph agree with theoretical resonance frequencies. As a general rule, the condition number may vary considerably from one problem to another,

and a stable value on the order of 1000 does not necessarily indicate a problem. However, any rapid change in the condition number is characteristic of a problem, and changes of the type depicted in Figure 6.3 are diagnostic of an interior resonance situation.

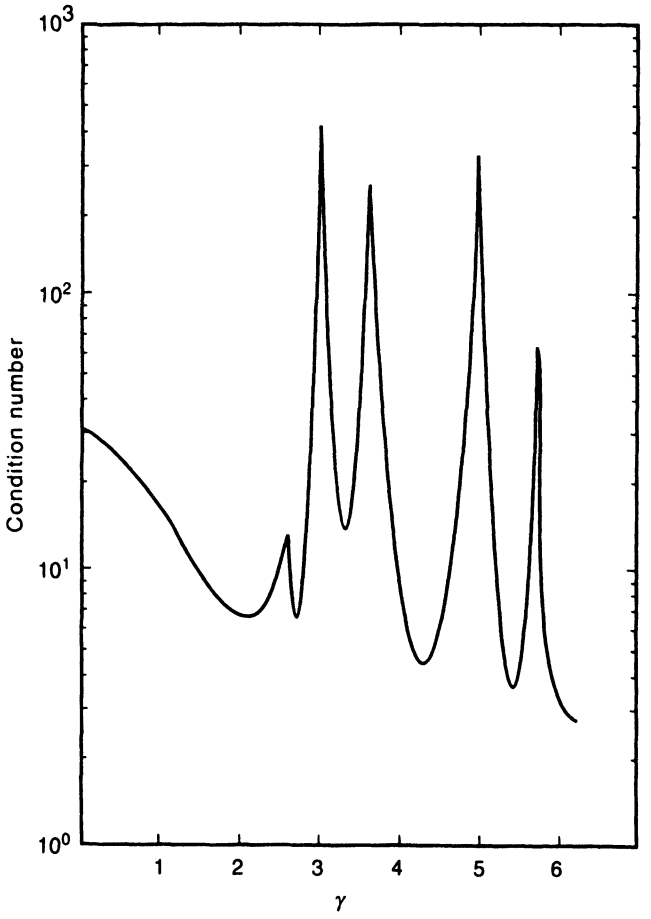

Figure 6.3 Plot of the matrix condition number of the system representing the TE MFIE for a circular cylinder of radius $a = 1$ as a function of the frequency parameter γ, where the circumference ka in wavelengths is given by $[(2\pi)^2 - \gamma^2]^{0.5}$. After [1]. ©1990 Hemisphere Publishing Corporation.

The relation between the resonant eigencurrent and the tangential incident field can be studied under general conditions using the reciprocity theorem [2] presented in Section 5.12, which can be written as

$$\iiint \bar{E}^a \cdot \bar{J}^b - \bar{H}^a \cdot \bar{K}^b = \iiint \bar{E}^b \cdot \bar{J}^a - \bar{H}^b \cdot \bar{K}^a \tag{6.10}$$

where the sources labeled a are located exterior to the scatterer and produce the incident fields associated with the exterior scattering problem (also labeled a). At a frequency where the scatterer surface coincides with the interior surface of a resonant cavity, the sources labeled b can be taken to represent any cavity eigencurrents. If the surface coincides with a cavity constructed of perfect electric walls (so that the tangential electric field vanishes on the surface), the magnetic current density $\bar{K}^b$ vanishes. Since $\bar{J}^b$ does not radiate outside

the cavity, it follows that

$$\iiint \bar{E}^{\text{inc}} \cdot \bar{J}^{\text{res}} = 0 \tag{6.11}$$

where $\bar{J}^{\text{res}} = \bar{J}^b$ denotes the resonant eigencurrent. If the scatterer surface coincides with a cavity constructed of perfect magnetic walls, a similar result is obtained involving the incident magnetic field and the resonant eigencurrent $\bar{K}^{\text{res}}$. These results demonstrate that the tangential component of the incident electromagnetic field will not excite the eigencurrent associated with the interior resonant cavity. This observation is in accordance with a mathematical principle known as the Fredholm alternative [3].

To summarize, numerical solutions of the surface EFIE or MFIE for closed scatterers may be incorrect near frequencies where the scatterer surface happens to represent a resonant cavity. Fundamentally, the problem is that the tangential components of a single incident field on the scatterer surface do not contain enough information to uniquely determine the desired surface currents at an interior resonance. Incorrect numerical solutions over a range of frequencies near resonance are caused by the improper balance between the small eigenvalue of the matrix and the corresponding term in the excitation vector. All the surface integral equation formulations discussed in Chapter 2 suffer from this problem, including those for homogeneous dielectric and impedance bodies (see Probs. P6.3 and P6.4). The volume integral equations do not suffer from this type of difficulty, since they sample the excitation throughout the interior region. Alternative surface integral equations are discussed in the following sections and can be used to avoid the internal resonance problem. We will see that each of these alternative formulations incorporates additional information about the incident fields present in the scattering problem. Unfortunately, they all require more computational effort than the EFIE or MFIE to produce the desired solution.

6.2 THE COMBINED-FIELD INTEGRAL EQUATION FOR SCATTERING FROM PERFECTLY CONDUCTING CYLINDERS [4, 5]

The preceding section described the basic interior resonance problem associated with the EFIE and MFIE. Not all surface integral equations suffer from this difficulty. An alternative formulation known as the combined-field integral equation (CFIE) provides unique, stable solutions for all closed scatterers [4, 5]. The CFIE is obtained from a linear combination of the EFIE and the MFIE. To scale terms to a similar order of magnitude and employ common units, the scale factors can be taken as α and $(1-\alpha)\eta$, where α is a real value between 0 and 1 and η is the intrinsic impedance of the exterior medium. The CFIE representing a perfectly conducting cylinder illuminated by a TM wave has the form

$$\begin{aligned}\alpha E_z^{\text{inc}}(t) + (1-\alpha)\eta H_t^{\text{inc}}(t) = (1-\alpha)\eta J_z(t) + \alpha jk\eta \int J_z(t')\frac{1}{4j}H_0^{(2)}(kR)\,dt' \\ -(1-\alpha)\eta \hat{t}\cdot\nabla\times\int \hat{z}J_z(t')\frac{1}{4j}H_0^{(2)}(kR)\,dt'\end{aligned} \tag{6.12}$$

where R is defined in Equation (6.2). For TE-wave scattering from perfectly conducting

cylinders, the CFIE is given by

$$\alpha E_t^{\text{inc}}(t) - (1-\alpha)\eta H_z^{\text{inc}}(t) = (1-\alpha)\eta J_t(t) + (1-\alpha)\eta \hat{z}\cdot\nabla\times\int \hat{t}(t')J_t(t')\frac{1}{4j}H_0^{(2)}(kR)\,dt' - \alpha\eta\hat{t}\cdot\frac{\nabla\nabla\cdot+k^2}{jk}\int \hat{t}(t')J_t(t')\frac{1}{4j}H_0^{(2)}(kR)\,dt' \tag{6.13}$$

The integrals in these equations are to be evaluated with the observer an infinitesimal distance outside the scatterer surface.

To illustrate the difference between these surface integral equations and the EFIE or MFIE, we again consider the special case of a circular cylinder with radius a. For the TE polarization, the eigenfunctions of the CFIE operator are $\{e^{jn\phi}\}$ and the corresponding eigenvalues are

$$\lambda_n^{\text{CFIE,TE}} = \tfrac{1}{2}(\eta\pi ka)H_n^{(2)\prime}(ka)[\alpha J_n'(ka) + j(1-\alpha)J_n(ka)] \tag{6.14}$$

A plot of the three dominant eigenvalues as a function of ka is presented in Figure 6.4 for $\alpha = 0.2$ and demonstrates that the eigenvalues never vanish. Consequently, the CFIE has unique solutions at all values of ka. The TM case exhibits similar behavior (Prob. P6.5).

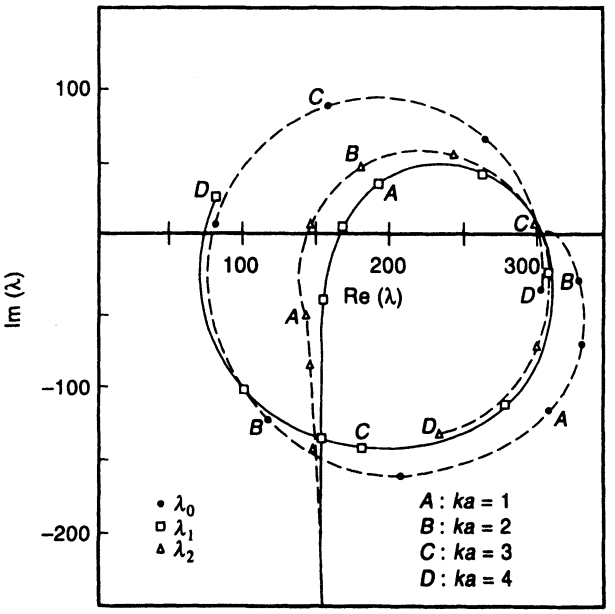

Figure 6.4 Plot of the three dominant eigenvalues of the TE CFIE as a function of ka. After [1]. ©1990 Hemisphere Publishing Corporation.

A more general uniqueness proof, adapted from [5], is as follows: Imposing Equation (6.12) in the absence of any incident field is equivalent to enforcing

$$\alpha E_z^s + (1-\alpha)\eta H_t^s = 0 \tag{6.15}$$

an infinitesimal distance inside the scatterer surface. By multiplying (6.15) with its complex

conjugate and integrating the result over the scatterer surface, we obtain

$$\int \mathrm{Re}[\bar{E}_z^s \times \bar{H}_t^{s\dagger} \cdot (-\hat{n})]\, dt = \frac{-1}{\alpha(1-\alpha)\eta} \int [\alpha^2 |E_z^s|^2 + (1-\alpha)^2 \eta^2 |H_t^s|^2]\, dt \tag{6.16}$$

The first expression in (6.16) is an integral over the time-averaged Poynting vector representing the flow of power into the scatterer interior, which must vanish. Consequently, if $\alpha \neq 0$ and $\alpha \neq 1$, then

$$E_z^s = 0 \tag{6.17}$$

and

$$H_z^s = 0 \tag{6.18}$$

an infinitesimal distance inside the scatterer. This demonstrates that the CFIE has no "interior-resonance" solutions unless $\alpha = 0$ or $\alpha = 1$ (in which case we are solving the MFIE or EFIE, respectively).

Furthermore, the excitation in Equations (6.12) and (6.13) involves incident tangential components of electric *and* magnetic fields. The combined excitation does not decouple from any of the eigencurrents as did the single type of excitation in Equations (6.8) and (6.9). As a result, the CFIE formulation involves sufficient information to uniquely determine the true surface currents for any nonzero value of ka.

We now consider a numerical implementation of the CFIE for the TM polarization. Suppose that the scatterer contour is represented by flat strips, as depicted in Figure 6.5. Normal and tangential vectors can be defined at the mth cell according to the angle Ω depicted in Figure 6.6, producing

$$\hat{n}_m = \hat{x} \cos \Omega_m + \hat{y} \sin \Omega_m \tag{6.19}$$

$$\hat{t}_m = -\hat{x} \sin \Omega_m + \hat{y} \cos \Omega_m \tag{6.20}$$

For pulse basis functions and Dirac delta testing functions, the method-of-moments matrix equation is of the form

$$\begin{bmatrix} C_{11} & C_{12} & \cdots & C_{1N} \\ C_{21} & C_{22} & \cdots & C_{2N} \\ \cdot & & & \cdot \\ \cdot & \ddots & \ddots & \cdot \\ \cdot & & & \cdot \\ C_{N1} & \cdots & \cdots & C_{NN} \end{bmatrix} \begin{bmatrix} j_1 \\ j_2 \\ \cdot \\ \cdot \\ \cdot \\ j_N \end{bmatrix} = \begin{bmatrix} e_1 \\ e_2 \\ \cdot \\ \cdot \\ \cdot \\ e_N \end{bmatrix} \tag{6.21}$$

The diagonal and off-diagonal entries are given by

$$C_{mm} = \frac{(1-\alpha)\eta}{2} + \frac{\alpha k \eta}{4} \int_{\text{cell } m} H_0^{(2)}(kR_m)\, dt' \tag{6.22}$$

and

$$\begin{aligned} C_{mn} = {} & \frac{\alpha k \eta}{4} \int_{\text{cell } n} H_0^{(2)}(kR_m)\, dt' \\ & + \frac{(1-\alpha)\eta j k}{4} \int_{\text{cell } n} \left[\sin \Omega_m \left(\frac{y_m - y'}{R_m} \right) + \cos \Omega_m \left(\frac{x_m - x'}{R_m} \right) \right] H_1^{(2)}(kR_m)\, dt' \end{aligned} \tag{6.23}$$

respectively, where

$$R_m = \sqrt{[x_m - x(t')]^2 + [y_m - y(t')]^2} \tag{6.24}$$

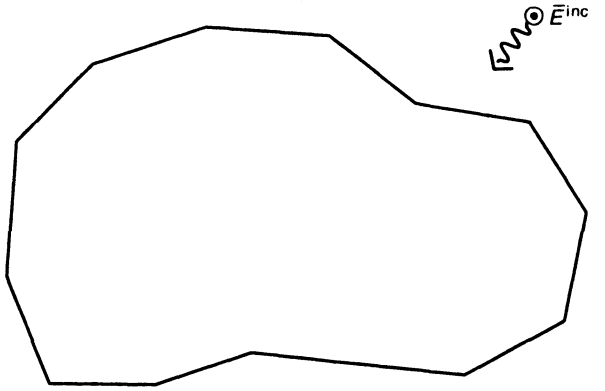

Figure 6.5 Flat-strip model of a cylinder cross section.

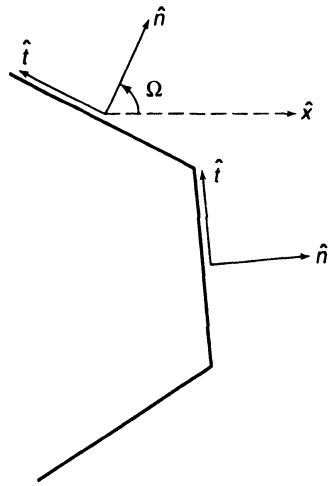

Figure 6.6 Tangent vector, normal vector, and polar angle Ω used to describe the orientation of the nth cell in the model.

If the incident field is a uniform plane wave propagating in the direction indicated by a conventional polar angle θ in the x–y plane, the entries of the excitation column vector are

$$e_m = [\alpha - (1 - \alpha)\cos(\theta - \Omega_m)]e^{-jk(x_m \cos\theta + y_m \sin\theta)} \tag{6.25}$$

These expressions involve integrals that are identical in form to those of the EFIE and MFIE discussed in Chapter 2, and their numerical evaluation is similar. From Equation (6.23), we see that two separate integrals are required for each of the off-diagonal entries of the matrix. Thus, although the CFIE guarantees unique solutions, the computational effort required to construct a matrix equation representing the CFIE is roughly double that required for the EFIE or MFIE alone.

Figures 6.7–6.12 illustrate the performance of the CFIE. Figure 6.7 shows the EFIE result for the current density induced by a plane wave on a circular cylinder with $ka = 5.15$ (near the theoretical TM_{21} cavity resonance). Clearly, the EFIE solution is completely incorrect (eigencurrents associated with the $e^{j2\phi}$ and $e^{-j2\phi}$ eigenfunctions are suppressed in the numerical result). For comparison, Figure 6.8 shows the CFIE result for the current density obtained with $\alpha = 0.7$ for the same cylinder. The CFIE formulation has eliminated the gross errors observed in the EFIE result. Figure 6.9 shows the scattering cross section for the circular cylinder example computed from the EFIE currents. Although in theory the far-zone fields should not be affected by the suppressed resonant current, some error is observed in the scattering cross section plot. (In this case, some discretization error may be present due to the relatively large cell sizes.)

As a second example and to illustrate the use of more general scatterer shapes, Figures 6.10 and 6.11 show the EFIE result for the current density induced by a TM wave on pie-shaped cylinders of similar electrical size. The currents of Figure 6.11 deviate significantly from the previous case and the physical optics solution, suggesting a possible interior resonance problem. Figure 6.12 shows the CFIE result obtained using $\alpha = 0.7$ for comparison to Figure 6.11. The CFIE solution exhibits good agreement with the physical optics solution and the solution of Figure 6.10, supporting our conjecture that the solution

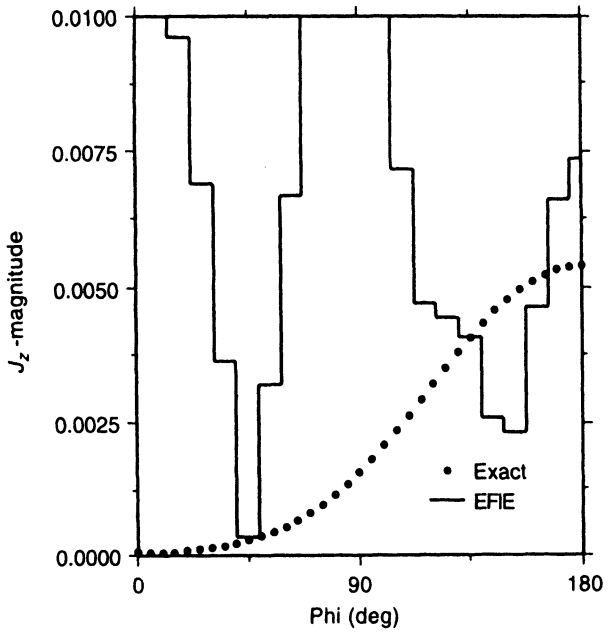

Figure 6.7 Comparison of the EFIE and exact solutions for the TM current density on a circular cylinder of radius $0.82\lambda_0$. The numerical result was obtained using 40 equal-sized cells.

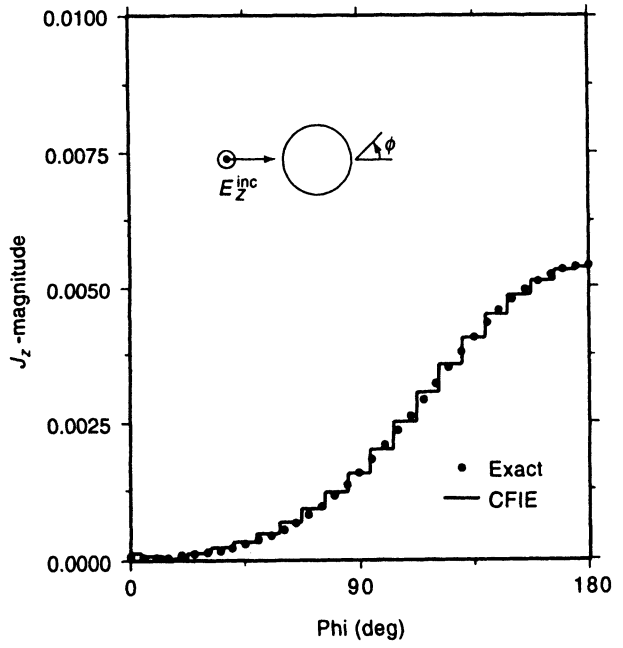

Figure 6.8 The CFIE result compared to the exact solution for the example of Figure 6.7. The CFIE parameter α equals 0.7.

of Figure 6.11 is corrupted by an interior resonance. For nonresonant pie-shaped cylinders, the CFIE result agrees with the EFIE solution.

In summary, the CFIE formulation can be used with perfectly conducting scatterers to produce the desired surface current density at all nonzero frequencies of interest. In ad-

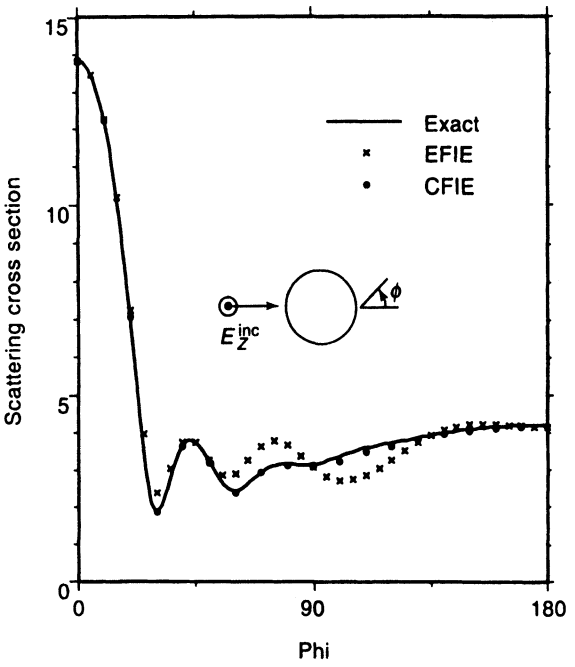

Figure 6.9 Two-dimensional scattering cross section produced by the EFIE result of Figure 6.7 compared with the exact solution and the CFIE result.

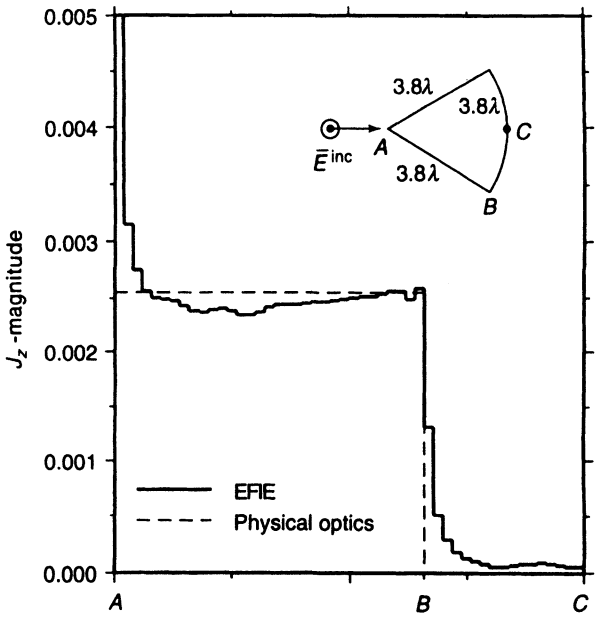

Figure 6.10 The EFIE result for the current density induced by a TM plane wave on a pie-shaped cylinder compared with the physical optics solution.

dition, the CFIE formulation is directly applicable to homogeneous dielectric scatterers and geometries incorporating an impedance boundary condition (Probs. P6.8 and P6.9). Since the matrix elements arising within the CFIE formulation are more complicated than those of the EFIE or MFIE, additional computational effort is required to implement the CFIE.

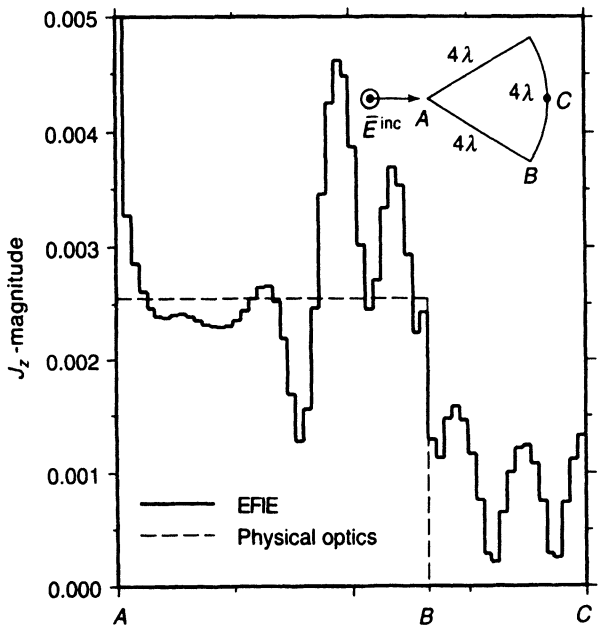

Figure 6.11 The EFIE result for the current density induced by a TM plane wave on a pie-shaped cylinder compared with the physical optics solution.

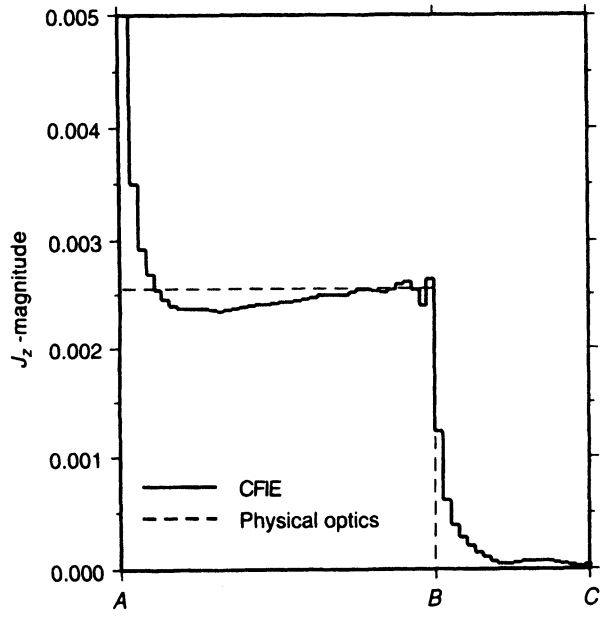

Figure 6.12 The CFIE result for the current density induced by a TM plane wave on the pie-shaped cylinder in Figure 6.11 compared with the physical optics solution.

6.3 THE COMBINED-SOURCE INTEGRAL EQUATION FOR SCATTERING FROM PERFECTLY CONDUCTING CYLINDERS [6, 7]

Integral equations are constructed by combining three factors: an equivalent mathematical source (electric or magnetic current density), a source–field relationship (expression for the field at some point in space in terms of an integral over electric or magnetic sources), and a

boundary condition on the surface of the scatterer under consideration (such as forcing the tangential $\bar{E}$-field at a perfect conductor to vanish). The EFIE, MFIE, and CFIE for perfectly conducting cylinders are formulated in terms of equivalent surface current densities

$$\bar{J} = \hat{n} \times \bar{H} \tag{6.26}$$

$$\bar{K} = \bar{E} \times \hat{n} = 0 \tag{6.27}$$

where $\bar{E}$ and $\bar{H}$ are the total fields external to the scatterer, $\bar{J}$ and $\bar{K}$ are the equivalent mathematical electric and magnetic surface current densities, and $\hat{n}$ is the outward normal vector along the scatterer surface. These equivalent sources are such that the correct fields are produced external to the scatterer and null fields are produced within the scatterer.

To model a perfectly conducting cylinder, it is natural to choose equivalent sources that, if used in connection with the complete set of boundary conditions, force the interior fields to vanish. However, the fields external to a scatterer can be correctly represented by many other equivalent sources, provided that the interior fields do not vanish. [Equations (6.26) and (6.27) are the only sources that produce zero interior fields and the correct exterior fields.] Since only the exterior fields are of interest, the interior fields can be arbitrarily chosen. This arbitrary choice allows a degree of freedom in the selection of equivalent sources, which may be taken to satisfy a constraint such as

$$\bar{K} = \frac{1-\beta}{\beta}\eta(\hat{n} \times \bar{J}) \tag{6.28}$$

for some real value of β between zero and one. It has been shown that this choice of equivalent sources may be used with perfectly conducting scatterers in order to remove the uniqueness problem from the original EFIE [6, 7]. This is possible because no eigencurrents associated with the interior cavity modes satisfy the additional constraint imposed by Equation (6.28).

The combined-source integral equation (CSIE) is constructed using the boundary condition that $\hat{n} \times \bar{E} = 0$ on the surface of the perfect electric conductor. For the TE polarization, the CSIE can be written as

$$\begin{aligned} \beta E_t^{\text{inc}}(t) = &-\hat{t} \cdot \frac{\nabla\nabla\cdot + k^2}{jk}\eta \int \hat{t}(t')\beta J_t(t')\frac{1}{4j}H_0^{(2)}(kR)\,dt' \\ &+ \hat{t} \cdot \nabla \times \int \hat{z}(1-\beta)\eta J_t(t')\frac{1}{4j}H_0^{(2)}(kR)\,dt' \end{aligned} \tag{6.29}$$

This equation is readily discretized into matrix form using the procedures discussed in Chapter 2. If specialized to a circular cylinder of radius a, the eigenvalues of this operator (associated with eigenfunctions $\{e^{jn\phi}\}$) can be found analytically to be

$$\lambda_n^{\text{CSIE,TE}} = \tfrac{1}{2}(\eta\pi ka)H_n^{(2)\prime}(ka)[\beta J_n'(ka) - j(1-\beta)J_n(ka)] \tag{6.30}$$

By analogy with Equation (6.14), it can be seen that these eigenvalues never vanish for real β between zero and one. In fact, for an appropriate inner product, the combined-source and combined-field operators are the adjoint of one another [7].

Although the combined-source formulation produces a unique solution, a drawback to the procedure is that the electric current density $\bar{J}$ in (6.29) is not the true electric current density induced upon the scatterer surface. In fact, since Equation (6.29) employs only the tangential incident electric field on the surface, it cannot produce the correct resonant eigencurrent associated with the exterior problem. Once the mathematical sources $\bar{J}$ and $\bar{K}$ are identified by solving (6.29), the true electric current density can be found from a

secondary calculation involving the incident magnetic field (Prob. P6.12). In common with the CFIE formulation, the tangential components of both the incident electric and magnetic fields must be employed in order to determine the true current density within a CSIE formulation. The matrix equation resulting from a method-of-moments discretization of the combined-source equation is of the same order and complexity as the matrix representing the combined-field integral equation.

6.4 THE AUGMENTED-FIELD FORMULATION [8]

The EFIE, MFIE, CFIE, and CSIE formulations involve boundary conditions imposed on the tangential components of the fields on the surface of a scatterer. As discussed, the tangential electric field or magnetic field alone is insufficient to determine the correct surface current density at resonant frequencies. Alternate surface integral equations have been proposed involving both the tangential and normal components of a single type of field [8]. These equations enforce the complete set of boundary conditions associated with the particular field and involve enough information about the incident field to uniquely determine the surface currents, except in a few exceptional situations. These "augmented-field integral equations" have the advantage over the CFIE formulation that the matrix elements are only as complicated as the original EFIE or MFIE formulations. However, when reduced to a matrix form using the method of moments, the system of equations is overdetermined by factors of 2 in two dimensions and $\frac{3}{2}$ in three dimensions. A special solution algorithm and additional computational time and storage beyond that of the original EFIE and MFIE will be required to solve the overdetermined system.

The augmented-field formulation will be illustrated in Chapter 8, when considering the problem of scattering from infinite cylinders illuminated from oblique angles.

6.5 OVERSPECIFICATION OF THE ORIGINAL EFIE OR MFIE AT INTERIOR POINTS

Since the basic interior resonance problem is the presence of fields interior to the scatterer geometry at discrete eigenfrequencies, a conceptually straightforward solution to the problem is the direct enforcement of a boundary condition throughout the interior region. This approach would necessarily involve the incident field within the scatterer and circumvent the difficulty associated with the tangential incident field on the scatterer surface decoupling from the resonant eigencurrent. A variety of proposed remedies have been based on variations of this idea [9–14], and we will not consider all of these in detail. A relatively simple approach has been proposed by Mittra and Klein, who suggest enforcing the condition that the E-field or H-field vanish at a variety of points within the scatterer geometry [10]. Although their original procedure requires the overspecification of the boundary conditions and the consequential solution of an overdetermined matrix equation, it is straightforward to add unknowns to balance the additional match points [12]. The latter idea has the potential advantages that the equation is no longer overdetermined and feedback concerning the interior current density (which should vanish if a "good" solution is obtained) is readily available. In addition, only the scatterer model is changed, so that existing computer codes based on the EFIE or MFIE may not need to be modified.

Consider Equation (6.1), the EFIE for TM scattering from perfectly conducting cylinders. Theoretically, this equation suffers from uniqueness problems associated with the TM modes of a perfectly conducting cavity, since the internal cavity fields satisfy the boundary condition imposed on the tangential electric field at the scatterer surface. In order to suppress these cavity fields, consider augmenting the scatterer model (originally consisting of strips located on the desired scatterer surface) with additional perfectly conducting strips distributed throughout the interior. The idea is to employ interior strips to "short out" any interior fields that might otherwise be present. The incident field sampled at the interior match points provides additional information in order to properly determine the resonant eigencurrent.

To illustrate the performance of this approach, consider a wave normally incident on a circular cylinder having a circumference of 5.15λ (near the theoretical TM_{21} cavity resonance). The EFIE solution using pulse basis functions and Dirac delta testing functions is displayed in Figure 6.7 and exhibits considerable error due to the cavity resonance. (As discussed previously, the $e^{j2\phi}$ and $e^{-j2\phi}$ eigenfunctions are suppressed in the numerical result.) Figure 6.13 displays the result after the cylinder model was augmented with three additional interior strips whose locations were chosen using random numbers. The additional strips have completely eliminated the interior fields from the cylinder, without a large increase in computational effort. For this particular example, the procedure is much more efficient than the CFIE formulation discussed in Section 6.2.

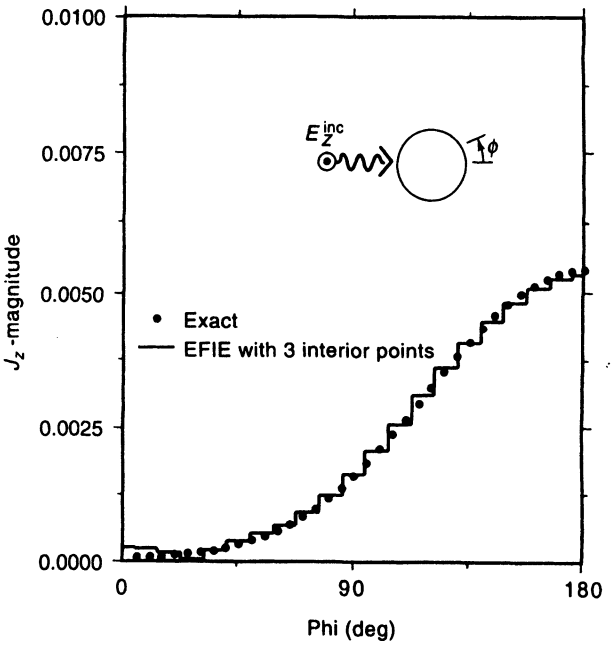

Figure 6.13 Comparison of the EFIE and exact solutions for the TM current density on a circular cylinder of radius $0.82\lambda_0$ after three interior strips were added to the model used to produce Figure 6.7.

The principal drawback to this type of remedy is the degree of user expertise required to determine the number of interior points and their precise location. Furthermore, the addition of a few interior strips may shift a resonance to a different frequency instead of completely eliminating it. Studies suggest that a uniform density of approximately 10 interior strips per square wavelength is necessary to completely suppress resonances in two-dimensional formulations [13]. Since the volume of the interior region increases faster than

the surface area, this approach appears to require the introduction of a prohibitive number of additional unknowns as the size of the scatterer increases relative to the wavelength. Although this simple procedure can be useful to eliminate resonances if encountered at single frequencies, it will prove to be less efficient for large scatterers than some of the other alternatives outlined in the preceding sections.

6.6 DUAL-SURFACE INTEGRAL EQUATIONS [14, 15]

The preceding section demonstrated that it is possible to enforce additional conditions inside the scatterer to eliminate the interior resonance problem. Unfortunately, the specific procedure of Section 6.5 generally requires user expertise and a large number of additional unknowns. Recently, a more systematic approach has been proposed that is convenient to apply and requires no additional unknowns [14, 15].

Consider Figure 6.14, which depicts a closed scatterer of perfect electric conducting material whose surface is denoted S_1. A second mathematical surface S_2 resides inside the scatterer. If equivalent electric surface current $\bar{J}$ is introduced on S_1 to replace the perfectly conducting material, a tangential-field MFIE may be expressed on the surface S_1 in the form

$$\hat{n} \times \bar{H}^{\text{inc}}(\bar{r}) = \bar{J}(\bar{r}) - \hat{n} \times \nabla \times \bar{A}\big|_{\bar{r}} \tag{6.31}$$

where $\bar{A}$ is the conventional magnetic vector potential due to $\bar{J}$ and $\bar{r}$ denotes a point approaching S_1 from the exterior. Equation (6.31) suffers from the interior resonance problem if S_1 happens to coincide with the interior of a resonant cavity having walls that are perfect magnetic conductors.

Since the total fields vanish everywhere inside S_1, an alternate tangential-field MFIE can be expressed on the surface S_2 in the form

$$\hat{n} \times \bar{H}^{\text{inc}}(\bar{r} - \bar{\delta}) = -\hat{n} \times \nabla \times \bar{A}\big|_{\bar{r}-\bar{\delta}} \tag{6.32}$$

where $\bar{r} - \bar{\delta}$ denotes an observation point on S_2. Note that the current density $\bar{J}$ used in (6.32) still resides on S_1. Equation (6.32) can produce correct solutions for $\bar{J}$ as long as S_2 does not coincide with the surface of a resonant cavity. However, consider the *dual-surface equation* obtained by combining Equations (6.31) and (6.32) to produce

$$\hat{n} \times \bar{H}^{\text{inc}}(\bar{r}) + \gamma \hat{n} \times \bar{H}^{\text{inc}}(\bar{r} - \bar{\delta}) = \bar{J}(\bar{r}) - \hat{n} \times \nabla \times \bar{A}\big|_{\bar{r}} - \gamma \hat{n} \times \nabla \times \bar{A}\big|_{\bar{r}-\bar{\delta}} \tag{6.33}$$

As long as the constant γ has a nonzero imaginary part, Equation (6.33) has unique solutions at all frequencies for which the surfaces S_1 and S_2 are separated by a nonzero distance of no more than approximately $\frac{1}{2}\lambda$ [14]. Furthermore, the unique solution is the desired exterior current density. Similar dual-surface equations can be derived based on an EFIE.

To illustrate that Equation (6.33) can eliminate the interior resonance problem, we again appeal to an eigenvalue interpretation possible with circular cylinders. Consider a circular cylinder illuminated by a TE wave. Suppose that the surface S_1 is circular with radius a and the interior surface S_2 is circular with radius $a - \delta$. If the dual-surface MFIE operator is defined to map functions on S_1 to functions on S_1, its eigenfunctions are of the form $e^{jn\phi}$ and the associated eigenvalues can be expressed for the TE case as (Prob. P6.13)

$$\lambda_n = \tfrac{1}{2}(j\pi ka)H_n^{(2)\prime}(ka)[J_n(ka) - \gamma J_n(ka - k\delta)] \tag{6.34}$$

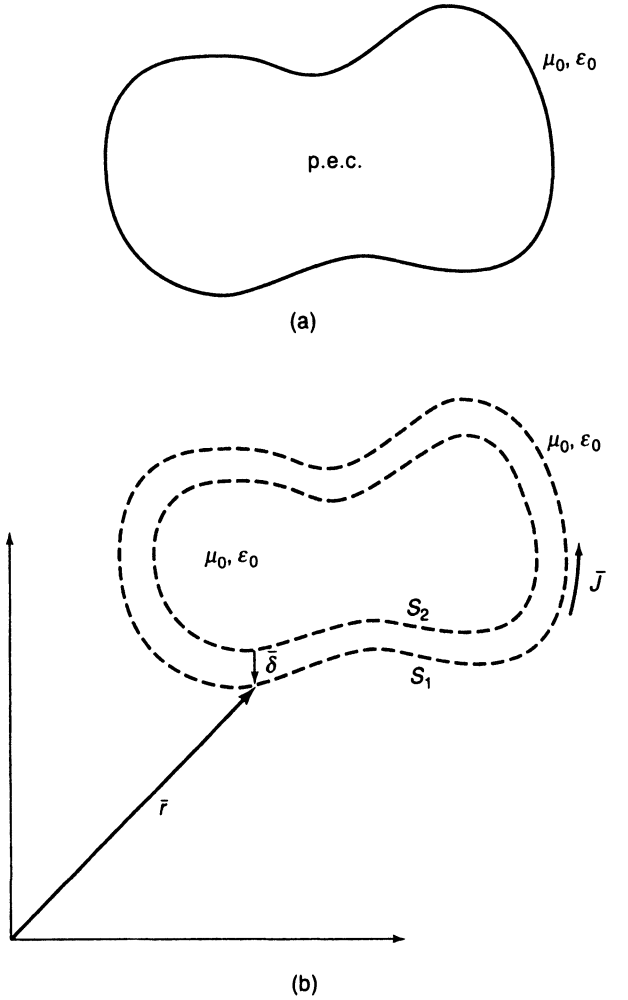

Figure 6.14 Geometry of a scatterer showing the dual surfaces S_1 and S_2.

As long as γ has a nonzero imaginary part, Equation (6.34) will not vanish unless $J_n(ka)$ and $J_n(ka - k\delta)$ vanish simultaneously. Since the zeros of $J_n(ka)$ occur at approximately half-wavelength intervals, it suffices to restrict the separation distance δ to less than that distance. (In practice, it would seem reasonable to separate S_1 and S_2 by $\frac{1}{4}\lambda$ whenever possible.)

Because the dual-surface equations sample the incident field on both S_1 and S_2, the incident field is not permitted to decouple from an individual eigenfunction (by restricting the separation distance between S_1 and S_2, we preclude the possibility that a single eigenfunction can vanish on both surfaces). In contrast to the CFIE or CSIE formulations, the dual-surface equations only require one type of integral operator (i.e., EFIE type or MFIE type), which may simplify the programming and the overall accuracy. The computational requirements to create the method-of-moments matrix are approximately twice that of the original surface integral equations. Since there are no additional unknowns, no extra computation is required for matrix solution beyond that of the conventional MFIE. The dual-surface equations are easily applied and appear to require no particular user expertise. If used over a range of frequencies, the location of S_2 must be adjusted to maintain the desired separation as a function of λ.

6.7 COMPLEXIFICATION OF THE WAVENUMBER [16, 17]

In theory, interior resonance solutions can only occur in a lossless environment. This raises the possibility of eradicating them by introducing a small amount of media loss. Unfortunately, loss sufficient to suppress resonances will also alter the desired solution to some extent. A procedure introduced in [16] avoids this problem by an extrapolation process and is easy to implement.

The idea is to solve the original EFIE or MFIE twice with enough medium loss in each case to suppress spurious interior resonances and use the two solutions to extrapolate to the lossless result. For instance, the real-valued wavenumber k can be replaced with $k_2 = k - j\delta$ and again with $k_1 = k - j\frac{1}{2}\delta$, where δ is typically on the order of a few percent of k. If the surface current densities obtained using k_1 and k_2 are denoted $\bar{J}_1$ and $\bar{J}_2$, a linear interpolation process similar to that used in Prob. P2.7 suggests that the surface current in the lossless case is approximately

$$\bar{J} \cong 2\bar{J}_1 - \bar{J}_2 \tag{6.35}$$

For better accuracy, three values of $\bar{J}_i$ can be obtained using three wavenumbers, and parabolic interpolation can be employed [17].

The "complexification" procedure can be successful as long as enough medium loss is incorporated to suppress spurious interior resonances. From the perspective of the circular cylinder examples considered in Section 6.1, the lossy medium changes the problematic factor $J_n(ka)$ to a Bessel function with complex argument, which no longer has zeros. Consequently, the incident field does not decouple from any of the matrix eigenvalues in the lossy case.

Compared with the original solution of the EFIE or MFIE, the procedure requires additional computation because of the need to solve two (or more) systems of equations. (As noted in [17], this computation can be alleviated to some extent if iterative techniques are employed to solve the equations, since the solution for one system can be used as the starting point for the next.) In addition, for the two-dimensional case, the procedure requires Hankel functions of complex argument, which are slightly more costly to compute than Hankel functions of real argument.

6.8 DETERMINATION OF THE CUTOFF FREQUENCIES AND PROPAGATING MODES OF WAVEGUIDES OF ARBITRARY SHAPE USING SURFACE INTEGRAL EQUATIONS [18–20]

In addition to treating scattering problems, the two-dimensional EFIE and MFIE can also be used to determine the cutoff frequencies of arbitrarily shaped waveguides. We have seen that the solutions to the surface integral equations are not unique at frequencies where the scatterer surface happens to coincide with a resonant cavity. Because the cutoff frequencies of the propagating modes are also the frequencies where the guides are two-dimensional resonant cavities, it is possible to use these equations to determine the cutoff frequencies and waveguide modes.

Consider a homogeneous waveguide with perfectly conducting walls. The TM cavity resonances of the corresponding infinite cylinder can be found using the EFIE of Equation (6.1), which we rewrite in the homogeneous form

$$\int J_z(t')H_0^{(2)}(k_c R)\,dt' = 0 \tag{6.36}$$

where R is defined in (6.2) and the integration is carried out over the interior surface of the cavity. In Equation (6.36), the current density $J_z(t)$ and the cutoff wavenumber k_c are unknowns to be determined. If the EFIE operator is converted to a method-of-moments matrix, the condition number or determinant of the matrix can be used to identify the wavenumber where the geometry supports a cavity resonance. This is a result of the fact that an eigenvalue of the matrix becomes relatively small near a cavity resonance. The method-of-moments matrix is a nonlinear function of the wavenumber, and generally an iterative or trial-and-error procedure must be employed to determine the wavenumber that minimizes the magnitude of the complex determinant or maximizes the condition number. (Because of discretization error, the determinant will usually not vanish.)

For illustration, Figures 6.15 and 6.16 show plots of the magnitude of the complex-valued determinant of the method-of-moments matrix as a function of the wavenumber k for triangular cavities modeled with 21 cells. The sharp dips in the determinant indicate resonant wavenumbers of the cavity. Figure 6.15 is based on an EFIE discretized according to the procedure described in Section 2.1, while Figure 6.16 is obtained from an MFIE formulation similar to that presented in Section 2.2. In order to use the MFIE to model a cavity with perfect electric walls, it is necessary to construct the method-of-moments matrix with the "outward" normal vector to the surface pointing *into* the interior of the cavity. (In the scattering problem discussed in Section 2.2 the normal vector points *out of* the closed scatterer. If the cavity surface was modeled with the normal vector pointing out,

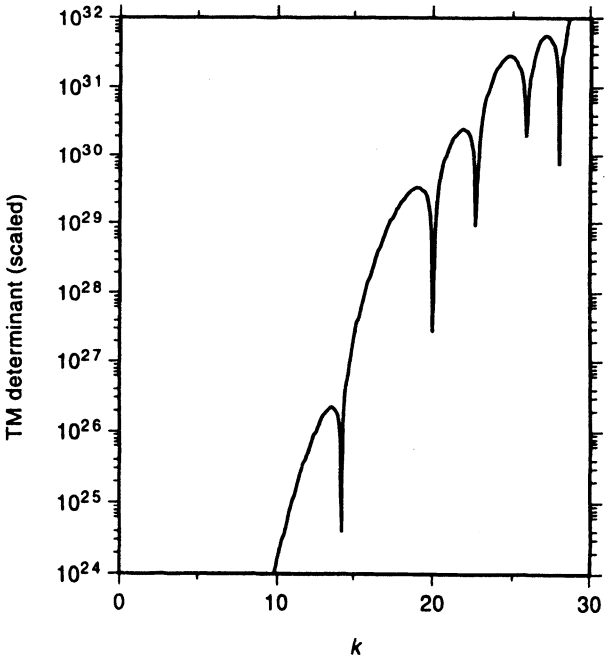

Figure 6.15 The EFIE result for the TM cutoff wavenumbers of a triangular-shaped cylinder. The triangle is right isosceles with side dimension 0.5. Sharp minima correspond to solutions of Equation (6.36).

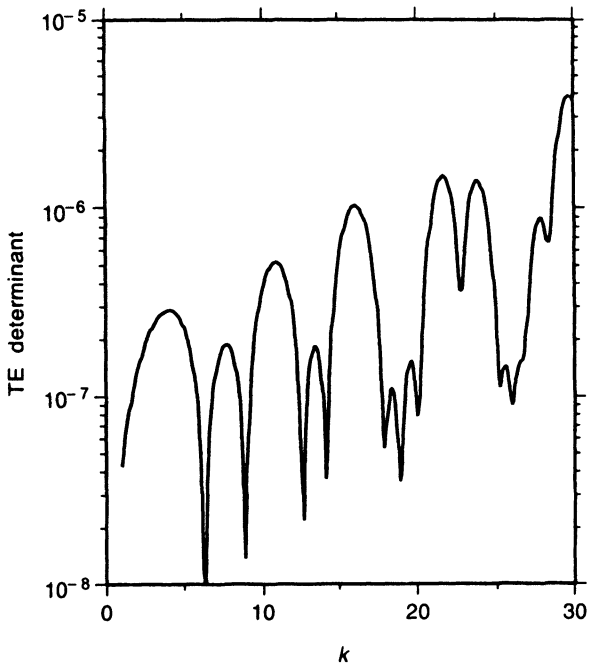

Figure 6.16 The MFIE result for the TE cutoff wavenumbers of a triangular-shaped cylinder.

the resonant frequencies obtained from the MFIE would be those for a cavity with perfect magnetic walls rather than perfect electric walls.)

Once the cutoff wavenumber is determined for a given mode, the current density can be found from the eigenvector of the method-of-moments matrix associated with the near-zero eigenvalue. The modal field distribution within the waveguide can be subsequently determined by an integration over the current density.

By combining surface integral equations for homogeneous dielectric regions with those for conductors, the idea described above can be extended to determine propagation constants in dielectric-loaded waveguides [19, 20]. A number of variations on the approach are possible, depending on whether the determinant, eigenvalues, or singular values of the matrix are to be computed and the degree of sophistication brought to bear on the problem of identifying the minimum values as a function of frequency. Because of the nonlinear behavior as a function of frequency and the need to construct the complete method-of-moments system at each frequency, the approach generally involves substantially more computational effort than a typical scattering problem. The complete characterization of a given waveguide may be time consuming.

6.9 UNIQUENESS DIFFICULTIES ASSOCIATED WITH DIFFERENTIAL EQUATION FORMULATIONS

In a lossless region, the scalar Helmholtz equation

$$\nabla \cdot \left(\frac{1}{\mu_r} \nabla E_z \right) + k^2 \varepsilon_r E_z = 0 \tag{6.37}$$

also admits homogeneous solutions when constrained by Dirichlet or Neumann boundary

conditions and is often used to find the resonant frequencies of closed cavities or the cutoff frequencies of waveguide modes. Consequently, if used with these boundary conditions within a scattering formulation, the Helmholtz operator may become highly ill-conditioned near frequencies where the interior region represents a resonant cavity.

Practical difficulties arise in connection with the so-called *inward-looking formulations* described in Section 3.12, since these employ Dirichlet or Neumann boundary conditions and attempt to solve (6.37) as the initial step of the procedure [21]. For illustration, Figure 6.17 shows a plot of the matrix condition number obtained from a discretization of (6.37) with Neumann boundary conditions for a circular region of free space having radius a. The scalar Helmholtz equation is discretized with piecewise-linear interpolation functions (Chapter 3) defined on a triangular-cell mesh with 85 nodes and 131 cells. Sharp spikes in the figure indicate resonant frequencies, which for this example correspond to the TM modes of an air-filled cavity with perfect magnetic walls.

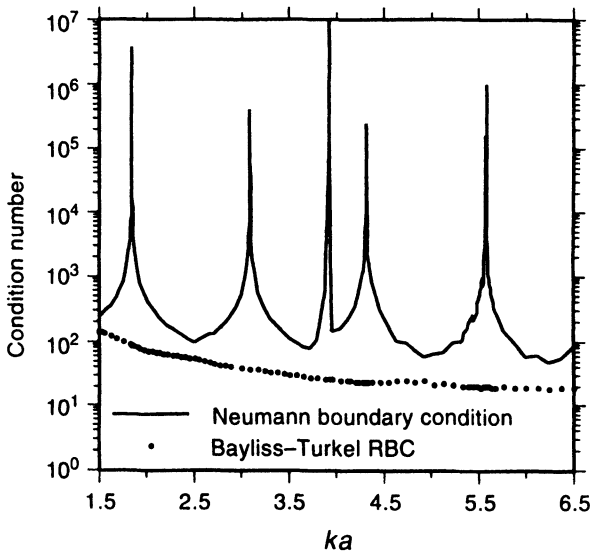

Figure 6.17 Matrix condition number for the system obtained from a discretization of the scalar Helmholtz equation for Neumann and Bayliss–Turkel boundary conditions. After [21]. ©1992 IEEE.

For comparison, Figure 6.17 also shows the matrix condition number when a local radiation boundary condition, the second-order Bayliss–Turkel RBC presented in Section 3.8, is used to constrain the scalar Helmholtz equation. Clearly, the radiation loss provided by the RBC is sufficient to eliminate any cavity resonances. Since the *outward-looking formulations* presented in Chapter 3 explicitly incorporate radiation loss, they are generally free of uniqueness difficulties arising from the scalar Helmholtz equation.

Outward-looking formulations that use either the EFIE or MFIE as an RBC (Section 3.10) remain vulnerable to internal resonance difficulties arising from the surface integral equations, however. As demonstrated previously, these formulations can be made robust by employing a CFIE as an alternative radiation boundary condition.

6.10 SUMMARY

The focus of this chapter has been the interior resonance problem and its remediation. Because of this difficulty, the conventional surface EFIE and MFIE are not recommended for analyzing closed-body scatterers large enough to support cavity resonant fields. Although

the internal resonance problem may not be encountered for every geometry of interest, there are certain situations where it is difficult or impossible to avoid. One such example is the case of a finite source illuminating an infinite cylinder, which can be treated by superimposing solutions obtained over a wide range of spatial frequencies. This procedure will be considered in Chapter 8 using some of the alternative formulations discussed in this chapter.

REFERENCES

[1] A. F. Peterson, "The interior resonance problem for surface integral equations of electromagnetics: Numerical consequences and a survey of remedies," *Electromagnetics*, vol. 10, pp. 293–312, 1990.

[2] R. F. Harrington, *Time-Harmonic Electromagnetic Fields*, New York: McGraw-Hill, 1961.

[3] D. H. Griffel, *Applied Functional Analysis*, New York: Wiley, 1981.

[4] K. M. Mitzner, "Numerical solution of the exterior scattering problem at eigenfrequencies of the interior problem," *Digest of the 1968 URSI Radio Science Meeting*, Boston, MA, International Union of Radio Scientists (URSI), p. 75, Sept. 1968. This conference digest not formally available from URSI.

[5] J. R. Mautz and R. F. Harrington, "H-field, E-field, and combined-field solutions for conducting bodies of revolution," Archiv für Elektronik und Übertragungstechnik (A. E. U.), vol. 32, pp. 157–163, 1978.

[6] J. C. Bolomey and W. Tabbara, "Numerical aspects on coupling between complementary boundary value problems," *IEEE Trans. Antennas Propagat.*, vol. AP-21, pp. 356–363, May 1973.

[7] J. R. Mautz and R. F. Harrington, "A combined-source formulation for radiation and scattering from a perfectly conducting body," *IEEE Trans. Antennas Propagat.*, vol. AP-27, pp. 445–454, July 1979.

[8] A. D. Yaghjian, "Augmented electric- and magnetic-field equations," *Radio Science*, vol. 16, pp. 987–1001, Nov. 1981.

[9] H. A. Shenk, "Improved integral equation formulation for acoustic radiation problem," *J. Acoust. Soc. Am.*, vol. 44, pp. 41–58, 1968.

[10] R. Mittra and C. A. Klein, "Stability and convergence of moment method solutions," in *Numerical and Asymptotic Techniques in Electromagnetics*, ed. R. Mittra, New York: Springer-Verlag, 1975.

[11] P. C. Waterman, "Numerical solution of electromagnetic scattering problems," in *Computer Techniques for Electromagnetics*, ed. R. Mittra, New York: Hemisphere, 1987 Reprint.

[12] A. F. Peterson and R. Mittra, "On the method of conjugate gradients for scattering by PEC cylinders," Electromagnetics Lab. Tech. Rep. 84-3, UILU-ENG-84-2540, University of Illinois, Urbana, IL, Jan. 1984.

[13] A. F. Peterson and R. Mittra, "Mutual admittance between slots in cylinders of arbitrary shape," Coordinated Science Lab. Tech. Rep., UILU-ENG-87-2247, University of Illinois, Urbana, IL, Aug. 1987.

[14] M. B. Woodworth and A. D. Yaghjian, "Derivation, application, and conjugate gradient solution of dual-surface integral equations for three-dimensional, multi-wavelength

perfect conductors," in *Application of Conjugate Gradient Method to Electromagnetics and Signal Analysis*, ed. T. K. Sarkar, New York: Elsevier, 1991.

[15] M. B. Woodworth and A. D. Yaghjian, "Multiwavelength three-dimensional scattering with dual-surface integral equations," *J. Opt. Soc. Am. A*, vol. 11, pp. 1399–1413, Apr. 1994.

[16] W. D. Murphy, V. Rokhlin, and M. S. Vassiliou, "Solving electromagnetic scattering problems at resonance frequencies," *J. Appl. Phys.*, vol. 67, pp. 6061–6065, May 1990.

[17] N. Engheta, W. D. Murphy, V. Rokhlin, and M. S. Vassiliou, "The fast multipole method (FMM) for electromagnetic scattering problems," *IEEE Trans. Antennas Propagat.*, vol. 40, pp. 634–641, June 1992.

[18] B. E. Spielman and R. F. Harrington, "Waveguides of arbitrary cross section by solution of a nonlinear integral eigenvalue equation," *IEEE Trans. Microwave Theory Tech.*, vol. MTT-20, pp. 578–585, Sept. 1972.

[19] M. Swaminathan, T. K. Sarkar, and A. T. Adams, "Computation of TM and TE modes in waveguides based on a surface integral formulation," *IEEE Trans. Microwave Theory Tech.*, vol. 40., pp. 285–297, Feb. 1992.

[20] S. Shu, P. M. Goggans, and A. A. Kishk, "Computation of cutoff wavenumbers for partially-filled waveguides of arbitrary cross-section using surface integral formulations and the method of moments," *IEEE Trans. Microwave Theory Tech.*, vol. 41, pp. 1111–1118, June/July 1993.

[21] L. W. Pearson, A. F. Peterson, L. J. Bahrmasel, and R. A. Whitaker, "Inward-looking and outward-looking formulations for scattering from penetrable objects," *IEEE Trans. Antennas Propagat.*, vol. 40, pp. 714–720, June 1992.

PROBLEMS

P6.1 Consider a perfectly conducting, circular cylinder with circumference ka illuminated by a TM or TE wave.

(a) A uniform TM plane wave can be expanded in a Fourier series

$$E_z^{\text{inc}}(\rho, \phi) = e^{-jkx} = \sum_{n=-\infty}^{\infty} j^{-n} J_n(k\rho) e^{jn\phi}$$

Assuming that the scattered field can be expressed as

$$E_z^s(\rho, \phi) = \sum_{n=-\infty}^{\infty} \alpha_n H_n^{(2)}(k\rho) e^{jn\phi}$$

find the exact solution to the scattering problem by determining the coefficients $\{\alpha_n\}$ in order to satisfy the boundary condition $E_z^{\text{tot}} = 0$ at $\rho = a$.

(b) Use the result of part (a) to show that the TM current density associated with the $n = 1$ harmonic $e^{j\phi}$ does not contribute to E_z^s when $J_1(ka) = 0$. What does this imply about the far-zone fields computed from the incorrect surface current density produced by the TM EFIE at an interior resonance?

(c) Using the TE plane wave

$$H_z^{\text{inc}}(\rho, \phi) = e^{-jkx} = \sum_{n=-\infty}^{\infty} j^{-n} J_n(k\rho) e^{jn\phi}$$

and the assumed scattered field

$$H_z^s(\rho, \phi) = \sum_{n=-\infty}^{\infty} \beta_n H_n^{(2)}(k\rho) e^{jn\phi}$$

find the exact solution by determining the coefficients $\{\beta_n\}$ that satisfy the appropriate boundary condition on H_z^{tot} at $\rho = a$.

(d) Use the result of part (c) to investigate the contribution to H_z^s from the TE current density associated with the $n = 1$ harmonic $e^{j\phi}$. Does this contribution vanish when $J_1(ka) = 0$ (at the interior resonance of the TE MFIE)? Discuss the implications.

(e) The eigenvalues presented in Equation (5.87) indicate that the interior resonance frequencies of the TE EFIE applied to a perfectly conducting circular cylinder occur at the zeros of $J_n'(ka)$. Would an incorrect $n = 1$ harmonic $e^{j\phi}$ produced by the TE EFIE contribute to the far-zone fields when $J_1'(ka) = 0$?

P6.2 Derive the reciprocity theorem used in Equation (6.10) by filling in the steps in the brief development presented in Section 5.12. Assume that sources $\bar{J}^a$ and $\bar{K}^a$ produce fields $\bar{E}^a$ and $\bar{H}^a$ and that sources $\bar{J}^b$ and $\bar{K}^b$ produce fields $\bar{E}^b$ and $\bar{H}^b$, when all the sources and fields exist in unbounded empty space. Clearly state necessary assumptions and restrictions. You may wish to review the similar development used in Equations (1.60)–(1.71) from Section 1.6.

P6.3 Consider a circular homogeneous dielectric cylinder of circumference ka illuminated by a uniform TM plane wave traveling in the x direction. The problem can be described by a coupled EFIE formulation, with equivalent currents $J_z(\phi)$ and $K_\phi(\phi)$ as primary unknowns (Section 2.8). In order to investigate interior resonance difficulties associated with this EFIE formulation, develop a method-of-moments discretization using the eigenfunctions $e^{jn\phi}$ as basis and testing functions and using the inner product

$$\langle a, b \rangle = \frac{1}{2\pi} \int_0^{2\pi} a^\dagger(\phi) b(\phi)\, d\phi$$

where $a^\dagger$ is the complex conjugate of a. Since the eigenfunctions of the integral operators are used as basis functions, the matrices will be diagonal. Show that the coefficients (j_n, k_n) associated with the nth cylindrical harmonic are described by the coupled equations

$$\alpha_n j_n + \beta_n k_n = e_n \qquad \gamma_n j_n + \delta_n k_n = 0$$

where

$$\alpha_n = \tfrac{1}{2}(\eta \pi ka) J_n(ka) H_n^{(2)}(ka) \qquad \beta_n = \tfrac{1}{2}(j \pi ka) J_n(ka) H_n^{(2)\prime}(ka)$$
$$\gamma_n = \tfrac{1}{2}(\eta_d \pi k_d a) J_n(k_d a) H_n^{(2)}(k_d a) \qquad \delta_n = \tfrac{1}{2}(j \pi k_d a) J_n'(k_d a) H_n^{(2)}(k_d a)$$

and

$$e_n = j^{-n} J_n(ka)$$

Discuss the implications of these equations with regard to possible internal resonance difficulties. What do these results suggest about the solution of similar EFIE formulations for noncircular cylinders?

P6.4 Consider a circular cylinder illuminated by a TM wave. Suppose that the cylinder is constructed from a material that can be characterized by a surface impedance boundary condition (IBC)

$$E_z(\phi) = \eta_s H_\phi(\phi) \quad \text{or} \quad K_\phi(\phi) = \eta_s J_z(\phi)$$

where η_s is the constant surface impedance. This problem can be described using the EFIE formulation discussed in Section 2.9. To investigate the interior resonance

difficulties associated with this surface integral, repeat the procedure from Prob. P6.3 in order to identify the entries of the matrix and the excitation vector associated with cylindrical harmonics. In general, will an interior resonance problem arise with this formulation? What does this observation suggest about the solution of similar IBC formulations for noncircular cylinders?

P6.5 By combining the results of Probs. P5.11 and P5.12, derive eigenvalues for the TM CFIE appearing in Equation (6.12) when applied to a circular conducting cylinder of radius a.

P6.6 Under what conditions will the TM CFIE matrix in Equation (6.21) exhibit symmetry across the main diagonal? How do the symmetry properties compare with those of the EFIE matrix developed in Section 2.1?

P6.7 Develop a method-of-moments discretization of the TE CFIE in Equation (6.13) using subsectional triangle basis functions and pulse testing functions (see the EFIE approach described in Section 2.4). Provide complete expressions for the matrix entries.

P6.8 Develop two different CFIE formulations for homogeneous dielectric cylinders illuminated by a TM wave. Use an appropriate combination of the surface integral equations appearing in (1.111), (1.112), (1.117), and (1.118) specialized to the TM case. (It is not necessary to provide a method-of-moments discretization of the resulting equations.) For the first CFIE formulation, use a linear combination of the two exterior equations to obtain a combined-field exterior equation similar to (6.12) and (6.13) and a linear combination of the two interior equations to obtain a combined-field interior equation. (Is the combined-field interior equation necessary for unique solutions?) For the second CFIE formulation, obtain one equation by enforcing continuity of the interior and exterior electric field and a second equation by enforcing continuity of the interior and exterior magnetic field. Can you think of any reasons why one of these approaches might be preferable to the other?

P6.9 Develop a CFIE formulation for TM scattering from cylinders described by a surface IBC. Identify the entries of the method-of-moments matrix if pulse basis functions and Dirac delta testing functions are used in the discretization in a manner similar to the Chapter 2 examples.

P6.10 Formulate a CSIE for TM-wave scattering from perfectly conducting cylinders of arbitrary shape. Develop a method-of-moments discretization using pulse basis functions and Dirac delta testing functions, and identify the entries of the method-of-moments matrix.

P6.11 Derive an expression for the eigenvalues of the TM CSIE when applied to a circular perfectly conducting cylinder of radius a.

P6.12 The equivalent current density $J_t(t)$ determined by a solution of the TE CSIE in Equation (6.29) is not the actual electric current induced upon the cylinder surface. Develop a procedure by which the true current can be determined once (6.29) is solved to produce $J_t(t)$.

P6.13 Verify Equation (6.34) using Equation (6.5) for the eigenvalues of the TE MFIE.

P6.14 Develop an MFIE formulation describing the TE cutoff frequencies for waveguides as discussed in Section 6.8. Provide entries for the method-of-moments matrix obtained using pulse basis functions and delta testing functions.